JOURNAL OF GEOPHYSICAL RESEARCH, VOL. 109, D06101, doi:10.1029/2003JD004012, 2004

Improved 11-year solar signal in the Freie Universität Berlin Climate Middle Atmosphere Model (FUB-CMAM)

Katja Matthes,[1] Ulrike Langematz,[1] Lesley L. Gray,[2] Kunihiko Kodera,[3] and Karin Labitzke[1]

Received 25 July 2003; revised 4 October 2003; accepted 24 October 2003; published 17 March 2004.

[1] So far, general circulation model studies have not been able to capture the magnitude and characteristics of the observed 11-year solar signal in the stratosphere satisfactorily. Here results from model experiments with the Freie Universität Berlin Climate Middle Atmosphere Model are presented that are in considerable agreement with observations. The experiments used realistic spectral solar irradiance changes, ozone changes from a two-dimensional radiative-chemical-transport model, and a relaxation toward observed equatorial wind profiles throughout the stratosphere. During Northern Hemisphere winter a realistic poleward downward propagation of the polar night jet (PNJ) anomalies, significantly weaker planetary wave activity, and a weaker mean meridional circulation under solar maximum conditions are reproduced in the model. The observed interaction between the Sun and the Quasi-Biennial Oscillation (QBO) is captured and stratospheric warmings occur preferentially in the west phase of the QBO. Only the magnitude of the anomalies during the dynamically active season improves, whereas the summer signal and the signal at low latitudes are still too weak. The results emphasize the important role of equatorial winds in achieving a more realistic solar signal by producing a more realistic wind climatology. Furthermore, they confirm recent results that equatorial winds in the upper stratosphere, the region dominated by the Semiannual Oscillation, are an important factor in determining interannual variability of the PNJ. *INDEX TERMS:* 1650 Global Change: Solar variability; 3362 Meteorology and Atmospheric Dynamics: Stratosphere/troposphere interactions; 3334 Meteorology and Atmospheric Dynamics: Middle atmosphere dynamics (0341, 0342); *KEYWORDS:* Sun-climate interactions, climate modeling, solar UV changes

Citation: Matthes, K., U. Langematz, L. L. Gray, K. Kodera, and K. Labitzke (2004), Improved 11-year solar signal in the Freie Universität Berlin Climate Middle Atmosphere Model (FUB-CMAM), *J. Geophys. Res.*, *109*, D06101, doi:10.1029/2003JD004012.

1. Introduction

[2] Understanding natural and anthropogenic contributions to climate change is an important issue in current observational and model studies. Natural variability from the Sun occurs over different timescales (e.g., 27-day rotational period, 11-year cycle, 88-year cycle, 200-year cycle, etc.) and possible Sun-atmosphere relationships have been of interest for a long time [e.g., *Bates*, 1981]. However, the understanding of the 11-year solar cycle influence on climate remained for a long time a difficult and controversial task [e.g., *Pittock*, 1978]. The aim of this paper is to investigate the role of the 11-year solar cycle and equatorial stratospheric winds on the atmosphere using a middle atmosphere climate model in order to get some insight into the mechanism of the solar influence on climate.

[3] Strong correlations between the 10.7 cm radio flux (as a measure for the 11-year solar cycle) and meteorological parameters such as temperature and geopotential height in the lower stratosphere (i.e., 100–30 hPa/~16–24 km) were first reported by *Labitzke* [1987] and *Labitzke and van Loon* [1988]. Initial observations of the upper stratospheric response to solar cycle ultraviolet (UV) changes [*Kodera and Yamazaki*, 1990] showed good correlations between the subtropical zonal mean wind at 1 hPa (~48 km) and the 11-year solar cycle. *Hood et al.* [1993] reported ozone, temperature, and zonal wind responses to solar UV changes in the upper stratosphere (i.e., 5–1 hPa/~36–48 km). These studies all used relatively short data sets preventing therefore statistically reliable results. However, recent studies confirm these earlier findings [e.g., *Labitzke*, 2001, 2002; *Kodera and Kuroda*, 2002; *Hood*, 2004].

[4] Possible mechanisms for the Sun-climate relationship include variations in the total solar irradiance (TSI), the UV spectral irradiance, the solar wind and the energetic particle flux. Variations in the TSI over one solar cycle are small

[1]Institut für Meteorologie, Freie Universität Berlin, Berlin, Germany.
[2]Centre for Global Atmospheric Modeling, Meteorology Department, Reading University, Reading, UK.
[3]Meteorological Research Institute, Tsukuba, Japan.

0148-0227/04/2003JD004012

(about ~0.1%) compared to the solar UV variations of ~5% at wavelengths from 200 nm to 300 nm which are important for ozone production and middle atmosphere heating [*Lean et al.*, 1997]. TSI changes alone seem to be not strong enough to explain a Sun-climate relationship, even though signals on decadal scales have been detected in upper ocean temperatures and attributed to the solar cycle [*White et al.*, 1997]. The correlation between cosmic rays and clouds [*Svensmark and Friis-Christensen*, 1997] is still a matter of debate. This paper will focus on 11-year solar UV changes.

[5] Since the advent of satellite instruments more accurate measurements of solar irradiance variations are available and the short-term UV variability has been well documented. Determination of the long-term UV variability requires several solar cycles. Presently, two solar cycles are well documented [e.g., *Lean et al.*, 1997]. It is known from past model studies that 11-year solar UV irradiance variations have a direct impact on the radiation and ozone budget of the middle atmosphere [e.g., *Brasseur*, 1993; *Haigh*, 1994; *Fleming et al.*, 1995]. During solar maximum (max) years the solar UV irradiance is enhanced, which leads to additional ozone production and heating in the stratosphere and above. By modifying the meridional temperature gradient the heating can alter the propagation properties for planetary and smaller-scale waves that drive the global circulation. Thus the relatively weak, direct radiative forcing of the solar cycle in the stratosphere could lead to a large indirect dynamical response in the lower atmosphere through a modulation of the polar night jet (PNJ) as well as through a change in the Brewer-Dobson circulation [*Kodera and Kuroda*, 2002]. Such dynamical changes can feedback on the chemical budget of the atmosphere because of the temperature dependence of the chemical reaction rates and transport of the chemical species. The transfer of the solar signal from the stratosphere to the troposphere is still not fully understood, although an influence on tropospheric circulation patterns was reported from model [e.g., *Haigh*, 1996, 1999; *Rind et al.*, 2002] as well as observational studies [e.g., *Labitzke and van Loon*, 1988; *Gleisner and Thejll*, 2003]. *Thompson and Wallace* [1998] showed that an annular mode, the Arctic Oscillation (AO), connects the atmosphere from the stratosphere down to the Earth's surface and *Baldwin and Dunkerton* [2001] as well as *Christiansen* [2001] recently showed the influence of stratospheric anomalies propagating to the troposphere. Possible interactions between the AO and its north Atlantic part, the NAO, with the solar cycle have been recently pointed out [*Kodera*, 2002] and could provide a mechanism through which the solar signal is transferred to the troposphere.

[6] A phenomenon that further complicates the identification of solar influences on climate is the Quasi-Biennial-Oscillation (QBO), which dominates the interannual variability of the equatorial stratosphere and influences higher latitudes significantly [e.g., *Baldwin et al.*, 2001]. *Holton and Tan* [1980, 1982] showed that the Arctic lower and middle stratosphere (i.e., 10 hPa/~32 km) tend to be cold and undisturbed during QBO westerlies (QBOw) while they are warm and disturbed during QBO easterlies (QBOe). *Labitzke* [1987] and *Labitzke and van Loon* [1988] confirmed these results but only for solar minimum (min) conditions. They showed further that during solar max years the so-called Holton and Tan (H&T) effect does not work and stratospheric warmings take place instead during the QBO west phase. New studies indicate that the QBO has a detectable influence even in summer: while the solar signal is very strong and significant during QBOe years, it is small and less significant during QBOw years [*Labitzke*, 2003]. The QBO-Sun relationship during winter was confirmed, for example, by *Salby and Callaghan* [2000]. Recently, *Gray et al.* [2001a, 2001b] showed that winds in the upper stratosphere, the region dominated by the Semiannual Oscillation (SAO), should not be neglected in determining interannual variability of the PNJ. They could only reproduce the H&T effect in a mechanistic model when they included equatorial winds up to 58 km (~0.3 hPa) height. Changes in the equatorial winds in the lower stratosphere alone were not able to reproduce the observed relationship. *Nastrom and Belmont* [1980] found that the amplitude of the SAO was 10–50% larger during solar max compared to solar min and that the period of the QBO varied inversely with the solar cycle. However, their database was very limited. Given that the strongest direct impact of the 11-year solar cycle appears around the equatorial stratopause [e.g., *Brasseur*, 1993; *Haigh*, 1994; *Fleming et al.*, 1995], an influence of solar irradiance changes on the SAO seems to be plausible. Through a coupling between SAO and QBO [e.g., *Garcia et al.*, 1997; *Garcia and Sassi*, 1999] the solar-induced wind changes could propagate downward.

[7] In order to confirm the observed relationship between the 11-year solar cycle and the atmosphere and to find the responsible mechanisms, general circulation model (GCM) studies, like the one presented here, are very useful. Early GCM simulations [e.g., *Wetherald and Manabe*, 1975; *Kodera et al.*, 1991; *Balachandran and Rind*, 1995; *Cubasch et al.*, 1997; *Balachandran et al.*, 1999] only used TSI or unrealistically large solar UV changes without considering the solar-induced ozone changes. They were able to simulate some of the characteristics of the observed atmospheric responses to the 11-year solar cycle, but failed to reproduce the observations quantitatively. Detailed GCM investigations using realistic spectral solar irradiance variations have only been possible in recent years [e.g., *Haigh*, 1999; *Shindell et al.*, 1999, 2001; *Larkin et al.*, 2000; *Matthes et al.*, 2003]. However, a comparison of these solar experiments [*Matthes et al.*, 2003] revealed that while the models simulate common features, such as a maximum heating of 1–2 K during solar max at the stratopause, they are not able to fully reproduce the magnitude of the observed solar signal, nor its annual and spatial propagation, indicating that some processes are either missing in the models, or not yet known. First results from GCM experiments with interactive chemistry [e.g., *Labitzke et al.*, 2002; *Tourpali et al.*, 2003] suggest that the interactively calculated ozone does not give a qualitatively different or better response than the GCM experiments using specified ozone. There still exist considerable discrepancies in the solar temperature signals in these models which are therefore not discussed in detail here.

[8] To date, none of the GCM simulations considers the QBO/SAO-Sun relationship. In this paper, we present the first simulation of a realistic QBO/SAO-Sun relationship. Our study used realistic spectral solar irradiance and ozone changes, which are equivalent to the solar intercomparison

Table 1. SW Radiation Schemes Used in the FUB-CMAM

Band	Gas	Wavelength, nm	Old Spectral Intervals	New Spectral Intervals
		Morcrette [1991]*Scheme*		
SW[a]	O_3	250–4000	2	2
		WMO [1986]/*Shine and Rickaby* [1989]		
Herzberg cont.[a]	O_2/O_3	206.186–243.902	2	15
Hartley bands[a]	O_3	243.902–277.778	2	10
Huggins bands[a]	O_3	277.778–362.500	3	18
Chappuis band[a]	O_3	362.500–852.500	1	1
		Strobel [1978]		
Schumann-Runge continuum	O_2	125–175	3	3
SR bands	O_2	175–205	1	1

[a]Wavelength interval adapted for the solar experiments.

study of the GCM-Reality Intercomparison Project for SPARC (GRIPS) [*Matthes et al.*, 2003]. New and different from these former experiments is the implementation of realistic equatorial wind profiles by a relaxation toward observed equatorial wind data throughout the stratosphere which improved the results significantly compared to former studies with the FUB-CMAM [e.g., *Labitzke and Matthes*, 2003] as well as compared to other GCM studies [e.g., *Matthes et al.*, 2003]. The paper is structured as follows: in section 2 the model and the experimental design are described, in section 3 the simulated response to the mean solar signal is investigated while the interaction between QBO and Sun is presented in section 4. The results are discussed in section 5 and summarized in section 6.

2. Model and Experimental Design

2.1. Model

[9] The Freie Universität Berlin Climate Middle Atmosphere Model (FUB-CMAM) is a spectral GCM, run with a horizontal resolution of $5.6° \times 5.6°$ (T21) and 34 vertical levels up to 0.0068 hPa (~83 km) [*Langematz and Pawson*, 1997; *Pawson et al.*, 1998]. The model thus includes the troposphere, stratosphere, and mesosphere with a distance of 3.5 km between adjacent layers in the middle atmosphere. The model physics [see *Pawson et al.*, 1998, and references therein] include the hydrological cycle, a full radiation scheme in the troposphere and middle atmosphere, vertical diffusion as well as a weak linear Rayleigh friction in the upper mesosphere, simulating the effect of gravity waves in a crude manner. In the basic model version [e.g., *Langematz*, 2000], the radiation scheme of *Morcrette* [1991] is used for absorption and emission of shortwave (SW) and longwave (LW) radiation due to ozone, water vapor, and CO_2. Above 70 hPa (~18 km) the absorption of UV and visible solar radiation due to O_3 and O_2 is calculated with the *Shine and Rickaby* [1989] scheme, and for O_2 with the *Strobel* [1978] scheme. At heights above 60 km (~0.2 hPa) a Newtonian cooling approximation is applied in the infrared.

2.1.1. Radiation Changes

[10] On the basis of observations from November 1989 for solar max and from September 1986 for solar min conditions, the spectral solar cycle variations were estimated in the wavelength interval 119.5 to 419.5 nm (resolution of 1 nm) [*Lean et al.*, 1997]. Before implementing these wavelength-dependent irradiance changes, the original resolution of the spectral bands in the *Shine and Rickaby* [1989] scheme was increased for the Herzberg, Hartley, and Huggins bands on the basis of *World Meteorological Organization* (*WMO*) [1986], leading to 44 instead of 8 spectral bands in the UV part of the spectrum (Table 1). Using the observed irradiance changes in the spectral bands from 200 to 420 nm, which contribute most to the SW heating in the stratosphere, the solar flux in the new radiation code was adjusted for solar max and solar min conditions. Differences in the absorption of visible light at the Earth's surface with the 11-year solar cycle were neglected, as the fixed SSTs did not allow to simulate a response to this effect. For computational efficiency, no changes were introduced in the *Strobel* [1978] scheme for the Schumann-Runge bands and the Schumann-Runge continuum (wavelengths shorter than 200 nm), because tests showed that the effect of 11-year solar irradiance changes on the absorption by molecular oxygen is negligible in the upper part of the model domain (the model lid is at 83 km/0.0068 hPa). The Lyman-α line (121.6 nm) was not included in the model's radiation code, hence effects from the high 11-year solar irradiance variability at 121.6 nm are neglected as they are only important for the upper mesosphere (above 75 km/0.02 hPa) and thermosphere. Consistent with the spectral solar irradiance changes, the TSI was also adjusted by 0.1% between solar max and min conditions [e.g., *Pap*, 2003] from a mean model value of 1367 W m^{-2}. Note that uncertainties exist for the estimated spectral solar irradiance changes because not all relevant processes (e.g., the origin of the 11-year solar cycle) in the Sun itself are fully understood and different assumptions and models are used to estimate these changes [e.g., *Pap*, 2003].

2.1.2. Ozone Changes

[11] The calculation of radiative heating rates in the FUB-CMAM version used for this study requires the prescription of an ozone distribution. Therefore the standard model ozone climatology (update of *Fortuin and Langematz* [1994]) was modified for solar max and min conditions. The solar cycle ozone changes were provided from a fully interactive two-dimensional (2-D) radiative-chemical-transport model [*Haigh*, 1994]. These data show 3% more ozone under solar max conditions between 10 and 5 hPa (32 and 36 km) depending on the season. Throughout the stratosphere the 2-D model produces more ozone during solar max years, in agreement with other model studies [e.g., *Brasseur*, 1993; *Fleming et al.*, 1995; *Shindell et al.*, 1999]

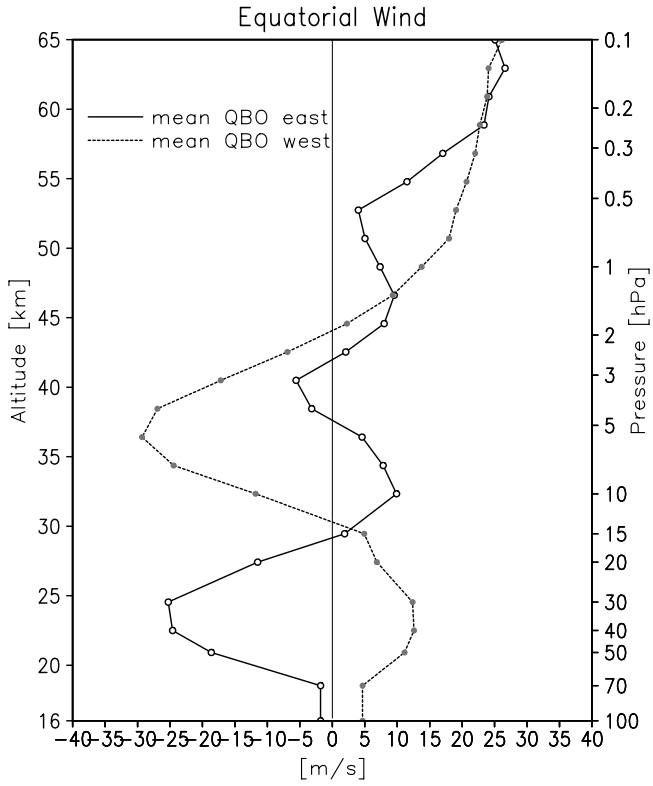

Figure 1. Mean equatorial wind profiles for QBO easterlies (solid) and QBO westerlies (dashed) constructed from rocketsonde data [*Gray et al.*, 2001b].

but in discrepancy with the Solar Backscatter Ultraviolet (SBUV) satellite measurements showing negative ozone changes in the middle stratosphere [*Hood*, 2004]. However, there is debate as to how the real solar ozone signal should be extracted from different data sets [e.g., *Hood*, 2004]. New studies with a fully interactive 2-D model [*Lee and Smith*, 2003] indicate that for an ozone solar signal similar to observations not only solar flux variations but also the effects of the QBO and volcanic eruptions have to be considered.

2.1.3. Equatorial Wind Profiles

[12] In the long-term mean state the FUB-CMAM, like most GCMs [e.g., *Pawson et al.*, 2000], is not able to reproduce a realistic QBO and shows instead weak easterlies in the equatorial lower stratosphere. It is however able to simulate the main features of the stratospheric SAO [*Müller et al.*, 1997], although the SAO easterlies are too strong, the westerlies are too weak and do not descend far enough down.

[13] To study the observed interaction between the QBO/SAO and the solar cycle during winter, the equatorial zonal winds in the model were relaxed toward idealized wind profiles. These were constructed by selecting profiles from rocketsonde data [*Gray et al.*, 2001b], which each had a QBO east phase (QBOe) in the equatorial lower stratosphere, a realistic shear zone in the middle stratosphere, i.e., a wind reversal at 10 hPa (on average observed around 10 hPa/32 km), and a SAO west phase (SAOw) in the upper stratosphere. The selected profiles were first averaged over a three month period (September to November) to exclude short term variations and then averaged to construct a mean wind profile for QBOe conditions in the lower stratosphere and SAOw conditions in the upper stratosphere (Figure 1). The same procedure was adopted to construct a mean QBOw profile. It should be emphasized that both idealized wind profiles (QBOe and QBOw) have a SAOw phase in the upper stratosphere. Only years from the rocketsonde data for solar min conditions were selected to avoid any solar preconditioning. The relaxation of the zonal wind is based on *Balachandran and Rind* [1995]. It extends latitudinally from 24.9°N to 24.9°S decaying with a Gaussian distribution centered at the equator. The vertical relaxation

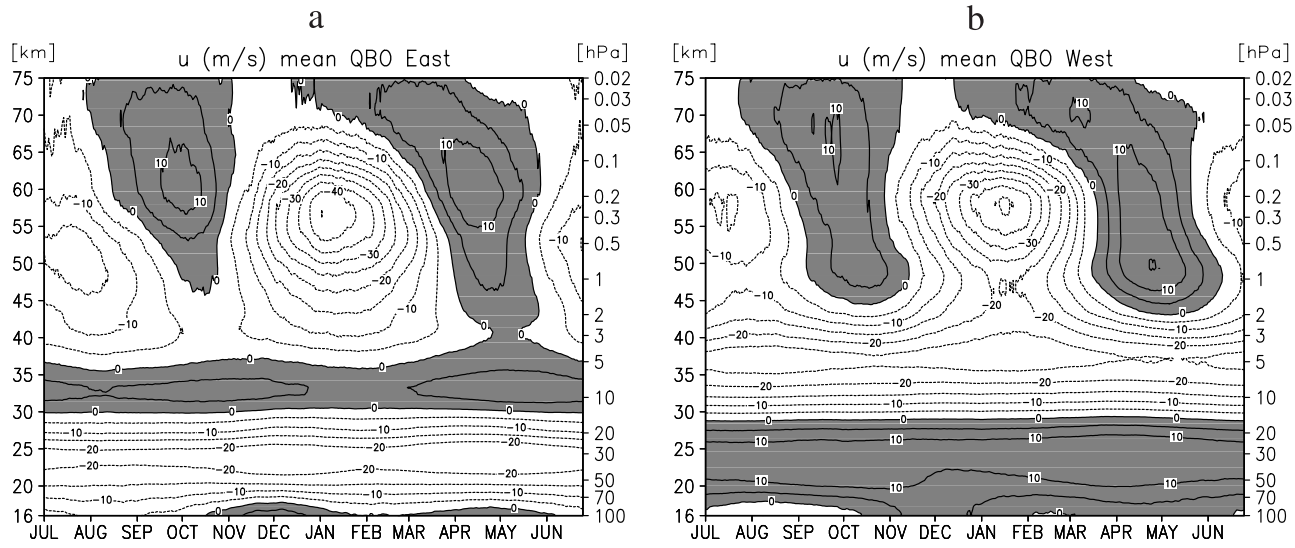

Figure 2. Long-term daily mean equatorial wind from the model after relaxation (averaged from 2.8°S to 2.8°N) from July until June for (a) mean QBOe and (b) mean QBOw in the equatorial lower stratosphere; west winds are shaded.

Table 2. Solar-QBO/SAO Experiments Performed With the FUB-CMAM

Experiment Name	Zonal Wind in Equatorial Lower Stratosphere	Solar Cycle Phase
maxW	west	maximum
minW	west	minimum
maxE	east	maximum
minE	east	minimum

extends from a height range of 18.4 to 66.0 km (~80 to 0.1 hPa). A relatively slow relaxation time constant of 20 days was employed, which constrained the equatorial winds to more realistic values while nevertheless allowing resolved equatorial waves to continue to propagate. Both of the imposed wind profiles (QBOe and QBOw) led to a weakening of the strong SAO easterlies and a strengthening of the SAO westerlies and hence to a more realistic SAO. The annual evolution of the climatological equatorial winds after the relaxation is shown in Figures 2a and 2b, respectively.

2.2. Model Integrations

[14] Four 15-year equilibrium runs (Table 2) were performed with the FUB-CMAM using changes in solar irradiance and ozone under perpetual solar max and perpetual solar min conditions, respectively, and for QBOe and QBOw conditions in the equatorial lower stratosphere (Figure 2). All experiments were integrated with an annual and diurnal cycle and employed climatologically varying SSTs, hence neglected highly variable phenomena such as ENSO at the lower model boundary. A comparison with previous 20-year equilibrium runs from the FUB-CMAM [e.g., *Labitzke and Matthes*, 2003] revealed that the statistical significances are robust in the tropics, subtropics and midlatitudes. The large interannual variability of the FUB-CMAM at high latitudes during winter prevents statistically significant signals for the 15-year integrations presented here, as well as for longer integrations.

[15] The experiments included neither a realistic time-varying 11-year solar cycle nor a realistic QBO with changes in sign of the equatorial winds or a descending of the wind regimes. Such experiments are beyond the current available computer resources as at least 100 years of integration are needed to achieve statistically reliable data. The generation of a realistic model-QBO would need sufficient spatial resolution, a gravity wave parameterization and a realistic simulation of tropical convection [e.g., *Giorgetta et al.*, 2002].

3. Solar Signal

[16] In this section we focus on the mean solar signal (hereafter referred to as "solar signal"), i.e., without separating the years according to the phase of the equatorial QBO, and investigate differences between solar maxima (max = (maxE + maxW)/2) and solar minima (min = (minE + minW)/2). All differences presented here are based on monthly mean data, averaged over 15 model years.

3.1. Annual Mean

[17] The SW heating rate difference (Figure 3a) supports results from other studies [e.g., *Brasseur*, 1993; *Haigh*, 1994; *Fleming et al.*, 1995; *Matthes et al.*, 2003] that the strongest direct solar effect is found in the stratopause region (around 48 km/1 hPa). Correspondingly, the strongest temperature response (Figure 3b) appears around the stratopause confirming the direct impact of the 11-year solar signal on temperatures in this height region. However, the

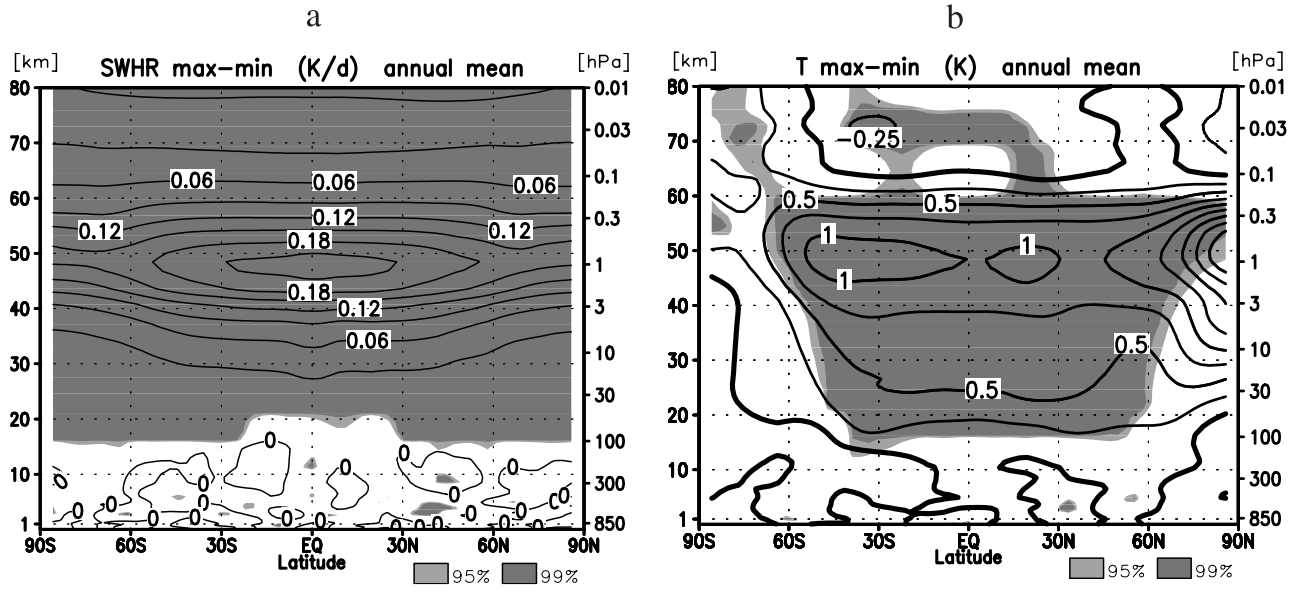

Figure 3. (a) Annual mean SW heating rate difference between 15 solar max and 15 solar min years in Kelvin per day (K d^{-1}); contour interval: 0.03 K d^{-1}. (b) Same as Figure 3a but for the annual mean temperature differences in K; contour interval: 0.25 K. Light (heavy) shading indicates the 95% (99%) significance level (Student's *t* test).

temperature and SW heating rate differences show different patterns. While the maximum SW heating rate change (0.22 K d^{-1}) occurs at equatorial latitudes the temperature change displays several maxima: one in southern midlatitudes (+1.1 K), one in northern subtropics (+1 K); the strongest temperature change at northern high latitudes (+2 K) indicates a strong dynamical feedback to the solar forcing in the model. Higher temperatures during solar max generally exist in a broad region from the upper atmosphere (60 km/~0.2 hPa) down to the surface from the north to the south pole. Whereas most of the stratospheric temperature signal is statistically significant, only small significant regions can be seen in the troposphere (between 30° and 60°N).

[18] Other GCM experiments performed so far [e.g., *Matthes et al.*, 2003] also imply the largest annual mean temperature response (about +0.75 to +1.2 K) near the stratopause. Using a 2-D chemical-dynamical-radiative model of the middle atmosphere, *Brasseur* [1993] calculates the strongest temperature signal of +1.4 K at 1 hPa (48 km) which decays with decreasing altitude similar to Figure 3b. The meridional structure of the temperature anomalies differs however from model to model.

[19] In the observations, the largest temperature signal of +0.8 K (derived from the Stratospheric Sounding Unit (SSU) data, 1979–1997) appears around 40 km (~0.3 hPa) and decays toward higher altitudes (0.4 K at 1 hPa/48 km) to even negative anomalies in the mesosphere [*Scaife et al.*, 2000]. A secondary temperature maximum occurs in the lower stratosphere (+0.25 K). In contrast, *Hood* [2004] derived a temperature signal from the National Centers for Environmental Prediction/Climate Prediction Center (NCEP/CPC) data (1980–1997) with a maximum of >2 K around the stratopause, slightly negative anomalies (−1 K) in the middle stratosphere, and a secondary maximum in the lower stratosphere (+1 K). This temperature pattern coincides with the derived solar cycle-induced ozone variation from the Solar Backscatter Ultraviolet (SBUV) data [*Hood*, 2004]. Another estimate of solar-induced temperature variations from rocketsondes [*Dunkerton et al.*, 1998] found a mean signal of +1.1 K averaged from 28 to 58 km (~15 to 0.3 hPa) and from 9°S to 38°N (the FUB-CMAM gives a value of ~0.8 K averaged from 8°S to 35°N and 27.5 to 57 km). In the NCEP/National Center for Atmospheric Research (NCAR) reanalysis data (1968–1998) *Labitzke* [2001] shows a maximum temperature difference of 1.5 K around 16 km (100 hPa). GCMs so far do not reproduce either the negative temperature signal in the middle stratosphere nor the secondary positive signal in the lower stratosphere.

[20] The discrepancies between the different data sets, for example, the negative temperature change pattern in the middle stratosphere derived by *Hood* [2004], which does not appear in the Scaife et al. data set, are due to the procedures adopted to extract the solar signal from the satellite instruments. Unfortunately, no data set covering the required altitude domain (troposphere, stratosphere, and mesosphere) and a sufficient time period in the stratosphere is so far available. So, while all models show a similar temperature signal around the stratopause, differences between modeled and observed signals are evident. However, as the observational estimates themselves diverge considerably in the upper stratosphere, a final conclusion on the quality of the simulated solar signal seems to be too early.

3.2. Northern Hemisphere (NH) Winter

3.2.1. Zonal Mean Temperature and Zonal Wind

[21] In Figure 4 the latitude-height distribution of zonal mean temperature and zonal wind differences is shown for the NH from October until March for the model (Figures 4a and 4b) and observations (Figures 4c and 4d) when the largest differences occur. In the model large temperature anomalies (Figure 4a) of different sign occur at high NH latitudes during winter whereas significant positive temperature anomalies dominate the tropical and subtropical stratosphere. The strongest effect on the latitudinal temperature gradient with a tropical warming and a strong, concurrent polar cooling occurs in early winter, i.e., November (Figure 4a). The quadrupol pattern of the temperature anomalies move downward from November until March with a period of 3 months. Because of the large year-to-year variability in the model at high latitudes in middle to late winter, polar latitudes show a significant signal only in October, while later in winter statistical significances are confined to lower latitudes as well as to the summer hemisphere (not shown).

[22] Simultaneously with the positive temperature anomaly in the equatorial upper stratosphere in October a statistically significant westerly wind anomaly of 2 m s^{-1} appears around 20°N and 55 km (~0.4 hPa) height which further grows and propagates poleward and downward with a period of 3 months (Figure 4b), similar to observations (Figure 4d). Under solar max conditions a stronger PNJ exists from November to January throughout the stratosphere. In January an easterly anomaly (−4 m s^{-1}) starts to propagate from the upper atmosphere poleward and downward until February (−10 m s^{-1}) and March (−16 m s^{-1}), which indicates the more frequent occurrence of stratospheric warmings during solar max. In January and February, only small statistically significant regions appear in the equatorial stratosphere and in the troposphere because of the large interannual variability in the model. In March the statistically significant regions grow again in the upper atmosphere at high latitudes as well as in large areas of the troposphere. At that time the variability in the upper stratosphere is lowered because of the spring warming of the Sun preceding the transition to summer conditions. Note that the anomalies extend down to the Earth's surface and are partly significant (e.g., in January and March).

[23] The pattern of simulated temperature and wind anomalies agree well with observations (Figures 4c and 4d) although the timing and the magnitudes are slightly different: The initial westerlies in the subtropical stratopause region appear in the model one month earlier (October) than in observations (November). The magnitude of the modeled anomalies (6 m s^{-1} in November) in mid latitudes is comparable to observations (4–8 m s^{-1} in December). However, the variability and therefore the magnitude of the differences at the subtropical stratopause region is smaller in the model; this is a typical GCM problem [*Kodera et al.*, 2003]. Therefore the initial westerly anomaly in October/November is much weaker in the model than in observations (12–14 m s^{-1} in December). The weaker model SAO west phase could be another explanation. In

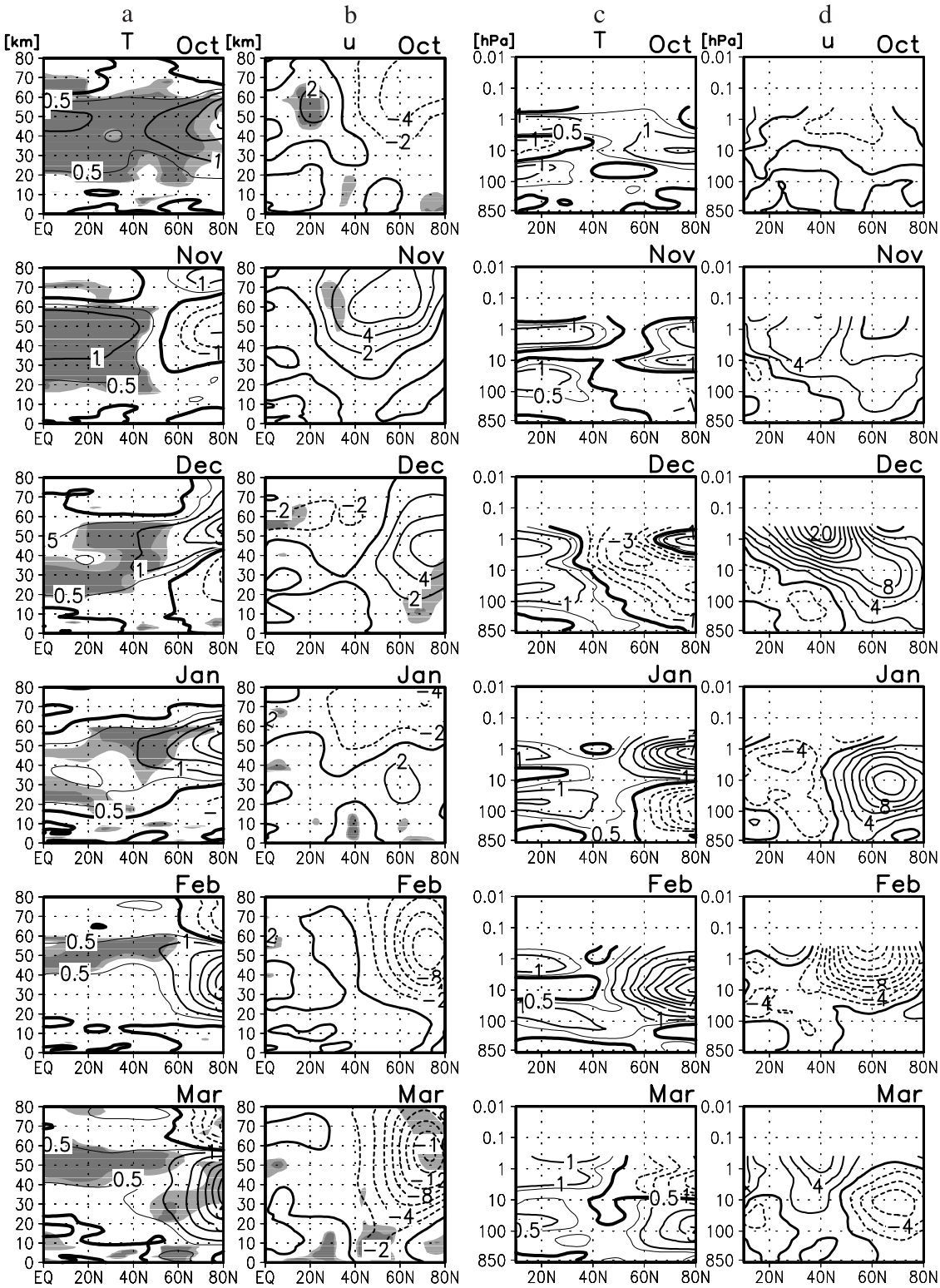

Figure 4. (opposite) Model results: (a) long-term mean temperature (contour interval: 1 K; 0.5 K contour line additionally plotted) and (b) wind differences between solar maxima and minima for the NH from October to March and the surface till 80 km (1000 to 0.01 hPa) (contour interval: 2 m s^{-1}). Shading is as in Figure 3. Observations as Figures 12 and 13 of *Kodera and Kuroda* [2002], except that October and March are added: (c) temperature differences between solar maximum (1979–1982 and 1988–1991) and solar minimum (1984–1987 and 1994–1997) years from NCEP-CPC data from 10°–80°N and 0–53 km (1000–0.5 hPa) (contour interval: 1 K, 0.5 K contour line additionally plotted), (d) as Figure 4c but for the wind differences (contour line: 2 m s^{-1}).

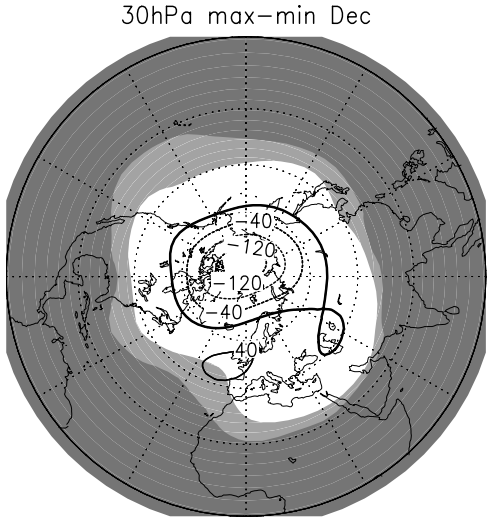

Figure 5. Long-term mean difference of the geopotential height at 30 hPa (∼24 km) for December; contour interval: 40 gpm. Shading is as in Figure 3.

general, the model differences occur at higher latitudes compared to observations. This is related to the strong upright PNJ (not shown). The secondary temperature maximum in the equatorial lower and middle stratosphere in observations is seen in the model only in January. A similar though slower poleward and downward movement of solar-induced zonal wind anomalies in the Southern Hemisphere (SH) [*Kuroda and Kodera*, 2002] is not reproduced in the model (not shown). We assume that this is due to the unrealistically strong PNJ during SH winter which suppresses small initial signals, for example, the solar signal, in early winter.

3.2.2. Geopotential Height

[24] Corresponding to the more realistic zonal mean wind response, the spatial pattern of the 30-hPa geopotential height differences, representative for changes in the lower stratosphere, has also significantly improved compared to earlier studies with the FUB-CMAM [*Labitzke and Matthes*, 2003] and other GCM studies [e.g., *Matthes et al.*, 2003]. The results are now in better agreement with observations. In Figure 5 we show the 30-hPa height differences for December, when the strongest PNJ changes occur (Figure 4b). Our results show that the polar vortex is 140 gpm deeper under solar max conditions whereas higher geopotential heights up to 40 gpm are found at lower latitudes. This is the typical seesaw pattern which has been observed [e.g., *Labitzke and van Loon*, 1988] and resembles the positive phase of the AO, i.e., a strong polar vortex. However, statistically significant regions are confined to lower latitudes. The modeled magnitude and structure of the height differences improve compared to earlier model studies [e.g., *Matthes et al.*, 2003] but in comparison with observations the magnitude is still substantially underestimated at low latitudes [*Labitzke*, 2003].

3.2.3. Possible Mechanisms

[25] The improved correspondence between modeled and observed solar signals during NH winter enables a detailed discussion of the dynamical processes. The anomalies of the Eliassen-Palm Flux vector (EPF) and its divergence (divF) (Figure 6a) show that the planetary wave propagation as well as the wave-mean flow interaction are influenced by the imposed solar irradiance changes.

[26] In November and December partly significant (not shown) positive anomalies of the EPF divergence are present in the middle and upper stratosphere from 30°N to 70°N (maximum of 2–2.5 m s^{-1} d^{-1} around 70°N and 54–

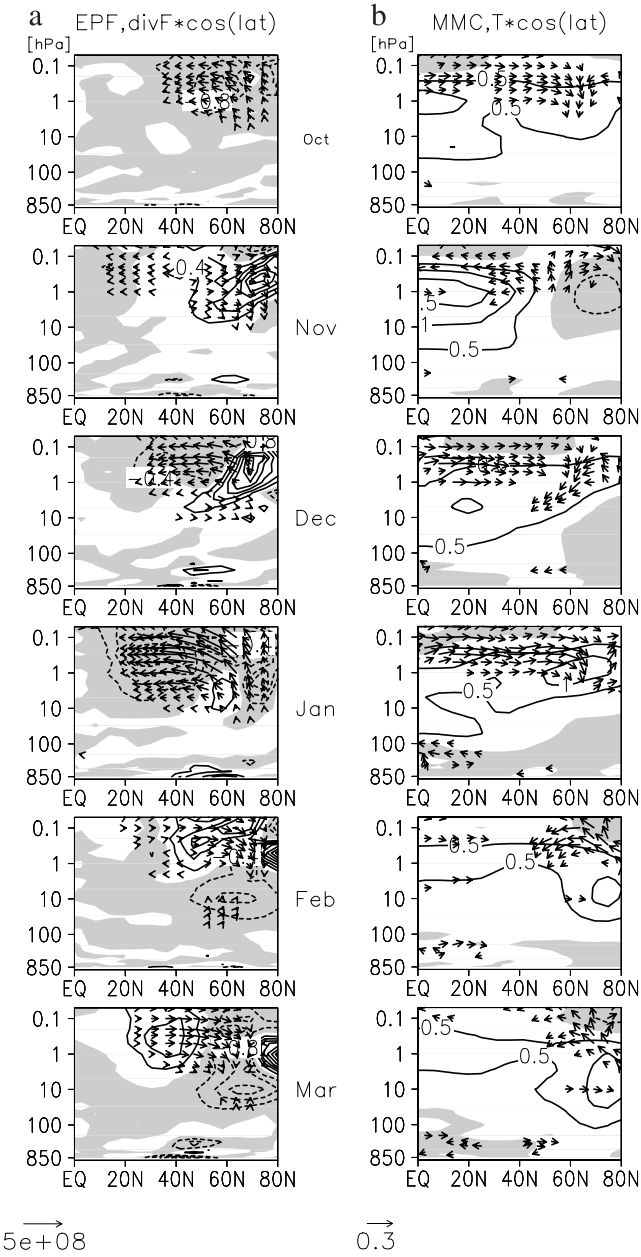

Figure 6. (a) Differences between solar maxima and minima in the EPF (arrows) scaled by the inverse of pressure to highlight the changes in the upper stratosphere and its divergence multiplied by cos(lat) (contour interval: 0.4 m s^{-1} d^{-1}); negative divergence anomalies are shaded from 1 to 70 km (850 to 0.05 hPa) and from the equator to 80°N for October to March. (b) Differences of the MMC (arrows) scaled as for the EPF anomalies in Figure 6a and of the zonal mean temperatures multiplied by cos(lat) (contour interval: 0.5 K); negative temperature anomalies are shaded.

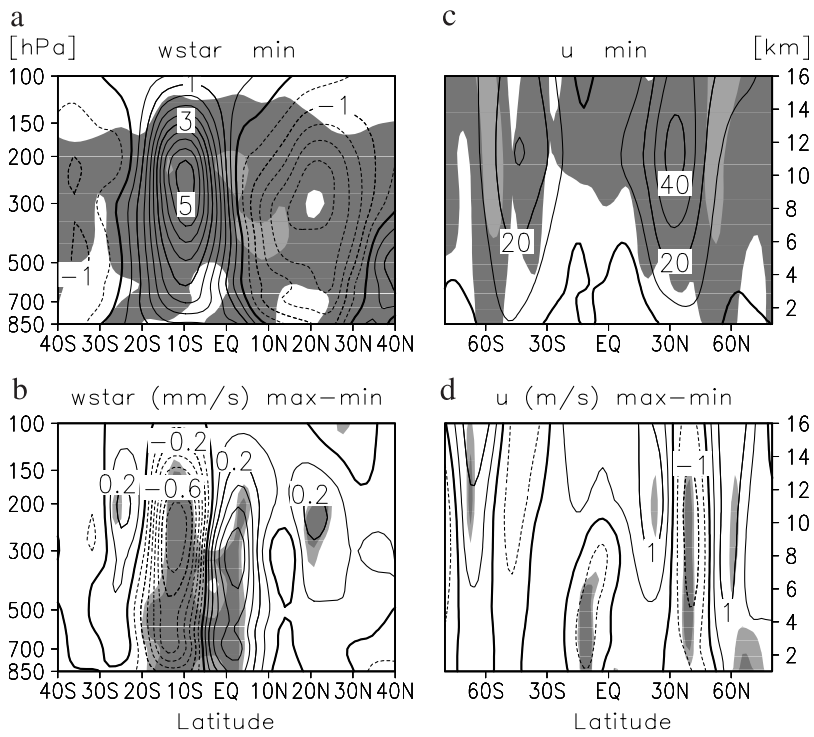

Figure 7. January: (a) Absolute values of the components of the MMC $\overline{w^*}$ (contours: 0.5 mm s^{-1}) and its standard deviation (shaded >0.2 and 0.4 mm s^{-1}) from 40°S to 40°N and 1 to 16 km (~850 to 100 hPa). (b) Difference between solar maxima and minima of $\overline{w^*}$ (0.1 mm s^{-1}); shading indicates statistically significant areas as in Figure 3. (c) Absolute values of the zonal mean wind (contours: 10 m s^{-1}) and its standard deviation (shaded >1 and 2 m s^{-1}) from 85°S to 85°N and 1 to 16 km (~850 to 100 hPa). (d) Wind difference between solar maxima and minima (0.5 m s^{-1}),; shading is as in Figure 3.

58 km/0.3–0.5 hPa). This implies a weaker wave-mean flow interaction hence weaker planetary wave activity under solar max conditions which is also seen in negative total heat flux anomalies at 100 hPa (16 km) (not shown) in agreement with estimates from observations [*Kodera and Kuroda*, 2002; *Hood*, 2004]. In November planetary waves propagate vertically upward and are reflected poleward in the vicinity of the westerly anomaly around 40°N in the upper stratosphere (Figure 4b), which itself strengthens. Therefore the dissipation of planetary waves, causing a deceleration of the zonal mean flow (positive anomalies of the EPF divergence in Figure 6a), takes place at higher latitudes and moves poleward and downward with time similar to the westerly wind anomaly. This positive feedback mechanism between planetary waves and the zonal mean wind anomaly is well known from observations [e.g., *Kodera and Kuroda*, 2002]. In January a negative subtropical wind anomaly in the upper stratosphere (Figure 4b) and a stronger significant convergence (−1.5 m s^{-1} d^{-1}) arise between 20° to 30°N and 35 to 70 km (~6 to 0.05 hPa) (Figure 6a). This coincides with larger EPF anomalies and strengthened planetary wave activity during solar max conditions. The stronger wave dissipation weakens the mean flow which enhances in turn the easterly wind anomaly: both effects reinforce each other.

[27] The weaker convergence at middle to high stratospheric latitudes in early winter (Figure 6a) leads to a weaker poleward Mean Meridional Circulation (MMC)

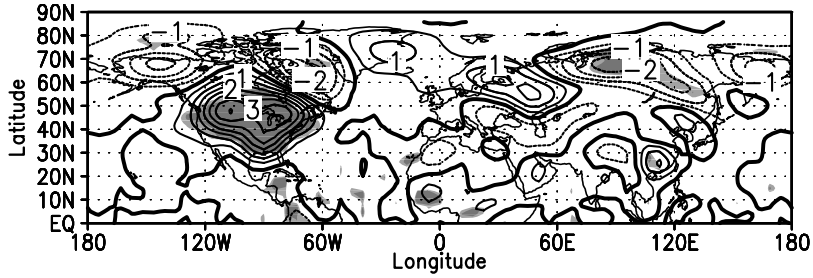

Figure 8. Surface temperature difference in February from the equator to 85°N and 180°W to 180°E; contour interval: 0.5 K; shading is as in Figure 3.

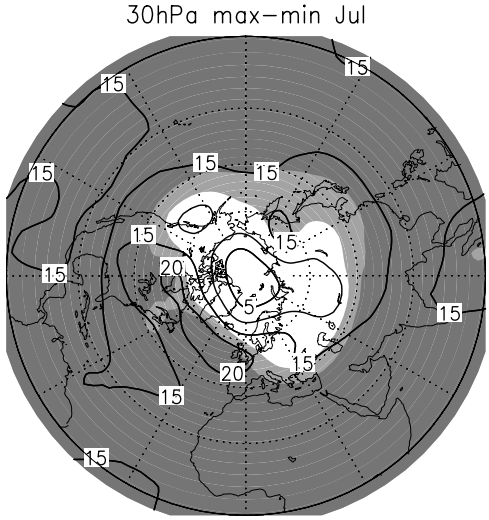

Figure 9. Same as Figure 5 but for NH summer (July); contour interval: 5 gpm.

(Figure 6b) at solar max conditions, i.e., a relative equatorward anomaly of the MMC, seen in November equatorward of 55°N in the upper stratosphere and in December at middle and high latitudes in the middle and upper stratosphere. This weakening of the global-scale MMC is associated with a relative warming of the tropical stratosphere (Figures 6b and 4a) which extends down into the lower stratosphere and upper troposphere from October until January. In January two statistically significant (see Figure 4b) maxima of the tropical temperature anomalies exist: one in the upper stratosphere around 1 hPa (48 km) and the other, equally strong, in the lower stratosphere (Figure 6b). This is comparable with observations from NCEP/CPC [*Hood*, 2004].

3.2.4. Tropospheric Changes

[28] One possible influence of the solar cycle on the troposphere is thought to originate from indirect circulation changes in the upper stratosphere [e.g., *Kodera et al.*, 1990; *Haigh*, 1996]. As already shown in Figure 4, stratospheric changes appear to impact the troposphere especially during NH winter. The strongest effect occurs in January (Figure 7) with a statistically significant weakening and broadening of the NH tropospheric jet (Figure 7d), whose core is located at 30°N and 12 km (200 hPa) (Figure 7c), during solar max. Concurrently, a statistically significant weakening and broadening of the ascending branch of the Hadley circulation around 10°S and a statistically significant weakening of the descending branch occur (Figures 7a and 7b). These results are in qualitative agreement with other model studies [e.g., *Haigh*, 1999; *Shindell et al.*, 1999, 2001; *Rind et al.*, 2002]. Although the annual mean temperature signal at the Earth's surface is negligible, there are nevertheless significant regional temperature differences at certain times of the year. Large and significant surface temperature anomalies appear over NH land masses which start to grow in December (not shown) and peak in February (Figure 8). Note that the surface temperature response is influenced by the fixed SSTs and can therefore only give a qualitative hint to tropospheric influences. We assume that the increasing tropospheric response from early to mid winter is connected to the poleward and downward movement of stratospheric circulation anomalies (see Figure 4) which affect the tropospheric circulation later in time: while the influence on the tropospheric jet is strongest in January, the influence on the surface temperature is strongest in February. A more detailed investigation of the reasons and mechanisms for the tropospheric signal will be subject of a future study.

3.3. NH Summer

[29] During NH summer, easterlies dominate the NH stratosphere and a dynamical coupling between the troposphere and stratosphere by planetary waves is prevented [*Charney and Drazin*, 1961]. Thus any influence of the 11-year solar cycle during summer can only operate via direct irradiance changes or via changes in the MMC resulting from dynamical coupling in the opposite (winter)

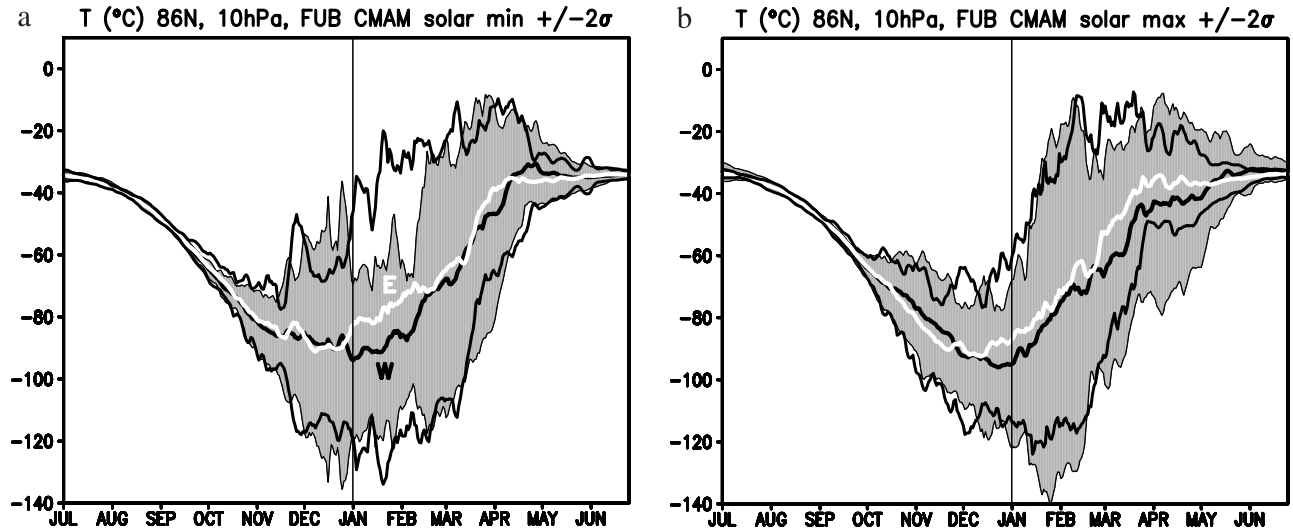

Figure 10. The 10-hPa (32 km) long-term daily mean NP temperature for solar (a) min and (b) max experiments. QBOw: black line with shaded 2σ standard deviation; QBOe: white line with open 2σ standard deviation. Vertical line in January to separate early and late winter.

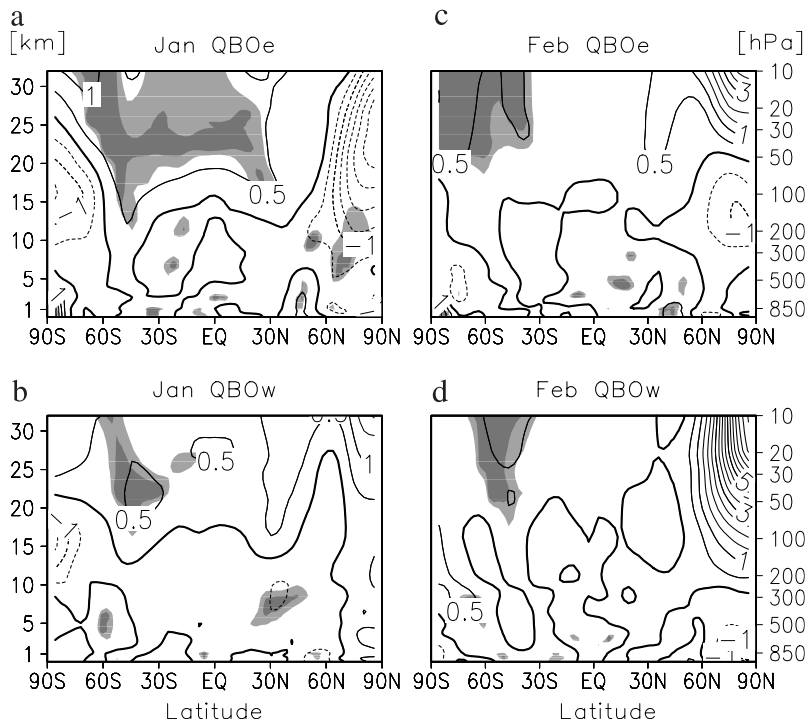

Figure 11. Temperature differences between solar max and min from 90°S till 90°N and 0 to 32 km (1000 to 10 hPa) for QBOe, (a) January and (b) February, and QBOw (c) January and (d) February; contour interval: 0.5 K; shading is as in Figure 3.

hemisphere. While in the study of *Labitzke* [2002] geopotential height differences of more than 80 gpm at 30 hPa (24 km) were derived in July/August, the simulated signal (Figure 9) only reaches +15 gpm in the subtropics, i.e., only 20% of the observed signal. Except for a small part of NH high latitudes the differences are statistically significant. Despite the anomalies being too weak, the overall pattern is reasonably captured in the model; that is, the strongest anomalies occur in the subtropics with higher geopotential heights from 20°S to 30°N, as is the movement of the strongest subtropical signal from one summer hemisphere to the other.

[30] We note that only the representation of the solar signal during the dynamically active season improves compared to other model studies [e.g., *Matthes et al.*, 2003] and is in better agreement with observations whereas the summer signal is still underestimated. This is also evident in the troposphere. While the strongest surface temperature anomalies range from +3 K to −2 K during NH winter (Figure 8), they are much smaller during NH summer (−1 to +1 K; not shown). This may be indirect evidence that the MMC changes are the dominant mechanism. As already noted, the SH responses are rather weak in winter, probably because of the rather strong PNJ in that hemisphere. Thus the weak solar response in the NH summer corresponds well to the weak MMC changes generated in the SH winter.

4. Interaction Between Solar and QBO Signals

[31] So far only the mean solar signal has been investigated. In this section the contribution of the dynamics in the tropical stratosphere (QBO/SAO) to the solar signal will be studied by analyzing both QBO phases separately for solar max and min conditions.

4.1. Zonal Wind–NH Winter

[32] *Labitzke* [1987] and *Labitzke and van Loon* [1988] pointed out that during NH winter the years should be separated into QBOe and QBOw years to detect the solar signal. Whereas during solar min years the H&T mechanism is evident, this is no longer the case during solar max years; here, major stratospheric warmings occur instead during QBOw years. For the first time, to our knowledge, this relationship has been reproduced in a GCM. Whereas the H&T mechanism is clearly evident for the solar min experiments, it is less clear for the solar max experiments as shown for the long-term daily mean 10 hPa North Pole (NP) temperatures in January and February (Figure 10). During solar min the NH polar stratosphere is colder in QBOw years (Figure 10a), while during solar max the occurrence of midwinter stratospheric warmings in QBOw years, as indicated by the stronger interannual variability in Figure 10b, leads to a comparable temperature evolution in both QBO phases. In the QBOw experiments (Figures 11c and 11d) stratospheric warmings associated with positive high-latitude temperature differences start to establish in January in the middle stratosphere and are clearly evident in February throughout the stratosphere reaching +8 K, in good agreement with the observed value of +9 K [*Labitzke*, 2001]. On the other hand, negative temperature differences indicating a colder and more undisturbed polar vortex are obvious in January throughout the stratosphere and in February in the lower stratosphere and upper troposphere for the QBOe experiments (Figures 11a and 11b). Positive temperature

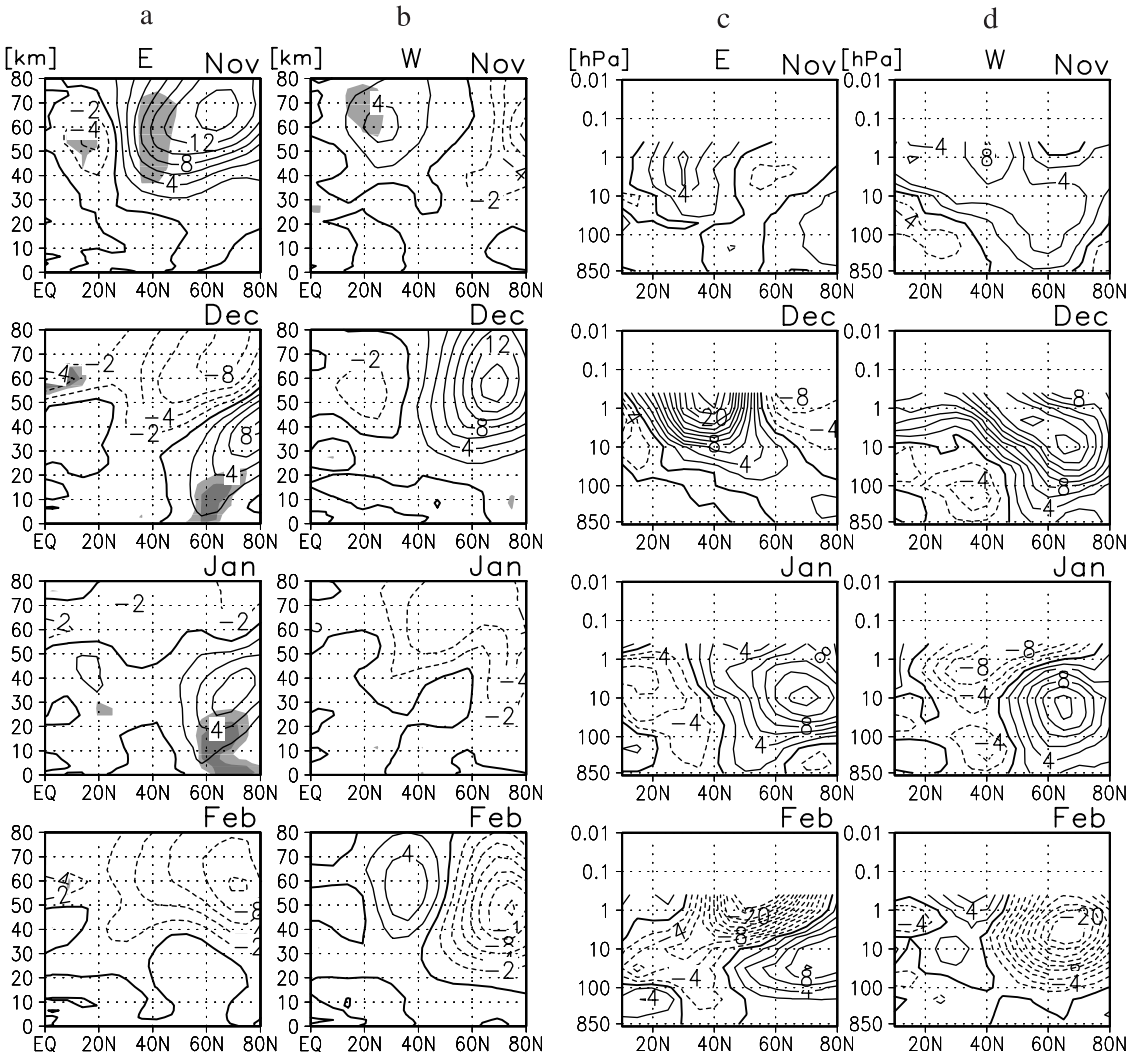

Figure 12. Model results: same as Figure 4b but for (a) QBOe and (b) QBOw experiment from November to February. Observations: same as Figure 4d but for (c) QBOe and (d) QBOw years: QBOe (1979, 1981, 1989, 1991, 1984, 1986, 1994, and 1996) and QBOw (1980, 1982, 1988, 1990, 1985, 1987, 1995, and 1997). The year corresponds to the month of December.

differences appear in the middle stratosphere in February for the QBOe experiments, i.e., 1 month later than for the QBOw experiments.

[33] The wind differences between solar max and min years from November to February shown separately for the QBOe and the QBOw experiments (Figures 12a and 12b) display a stronger magnitude of the differences compared to the wind differences of the mean solar signal (Figure 4b), for example, the large westerly anomaly of 14 m s^{-1} in November for the QBOe and in December for the QBOw experiment, in better agreement with observations (Figures 12c and 12d). In general, the anomalies in early winter are located more in the subtropics for the QBOe and more toward middle and high latitudes for the QBOw years in the model as well as in observations. In the model the overall development and movement of the zonal wind anomalies is very similar for both QBO phases (it is faster for the QBOw run and comparable to the mean solar signal for the QBOe run) indicating that the phase of the equatorial QBO only determines the temporal evolution of the solar signal. This confirms findings from observations (Figures 12c and 12d) despite the fact that the model response is shifted by about one month.

4.2. Geopotential Heights

[34] According to the largest difference in the PNJ between the QBOe and QBOw experiments in January, we show the geopotential height differences in the lower stratosphere for this month in Figure 13. For the QBOe case (Figure 13a) significantly lower heights at polar latitudes (−270 gpm) indicating a stronger polar vortex during solar max years and higher heights (+60/90 gpm) at mid latitudes are apparent. Note that the magnitude of the modeled height differences is enhanced compared to earlier model studies. Similar to the mean solar signal (Figure 5) the height differences resemble an AO positive pattern. For the QBOw case (Figure 13b) the signal is reversed, although less strong and nowhere significant. A weaker polar vortex appears for solar max conditions (+90 gpm) indicating the occurrence of stratospheric warmings and lower heights (−30 gpm) at

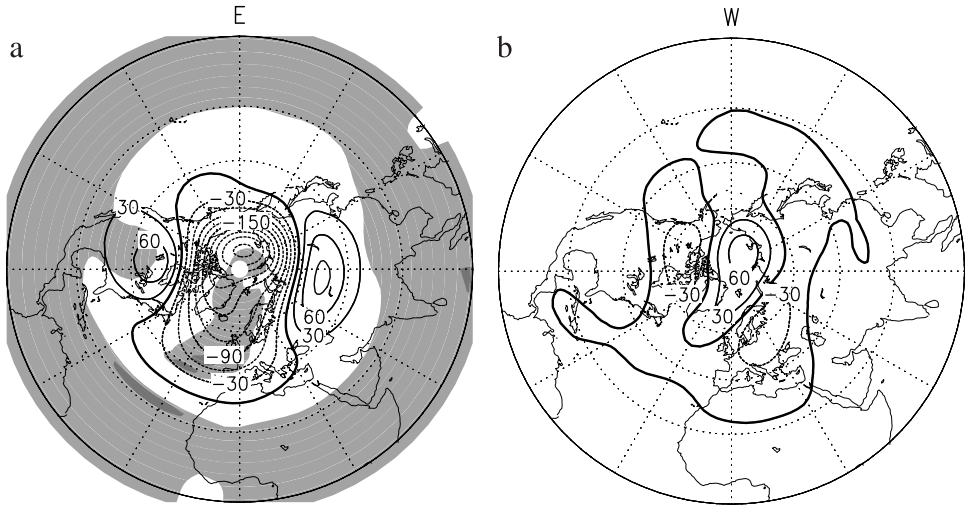

Figure 13. Long-term mean difference of the geopotential height at 30 hPa (~24 km) for January for (a) QBOe and (b) QBOw; contour interval: 30 gpm. Shading is as in Figure 3.

lower latitudes, resembling an AO negative signal. The more frequent occurrence of stratospheric warmings during QBOw and solar max years is in agreement with observations. However, the simulated magnitude is still too low compared with observed 30-hPa height differences in February [*Labitzke*, 2002].

[35] During NH summer, the simulated height differences for QBOe and QBOw (not shown) are still very low and no difference compared with the mean solar signal (Figure 9) could be detected. This supports our idea of a link between the strong SH PNJ and weak NH summer signals due to MMC changes generated in the winter hemisphere. A more detailed investigation of the QBO-Sun interaction will be subject of a future study.

5. Discussion

[36] The paper showed that the NH winter evolution has considerably improved compared to earlier studies with the FUB-CMAM [e.g., *Labitzke and Matthes*, 2003] and compared to other GCM studies [e.g., *Matthes et al.*, 2003] and is now in better agreement with observations [e.g., *Labitzke*, 2001; *Kodera and Kuroda*, 2002; *Hood*, 2004]. The temperature increase during solar max in the tropics and subtropics of the upper stratosphere can be explained via direct solar UV changes (Figures 3a and 3b) while dynamical effects (modulation of the PNJ and MMC, Figures 4 and 6) play an important role at middle and high latitudes of the stratosphere. The largest direct temperature effect on the winter hemisphere appears for both hemispheres in early winter, a period that is very sensitive to perturbations, for example, from solar UV radiation. Consistent with the direct temperature effect significant zonal mean wind anomalies appear slightly shifted upward (Figure 4). We conclude that changes in solar irradiance lead to changes in planetary wave propagation, hence wave-mean flow interaction and changes in the MMC in the stratosphere which are transferred to the lower atmosphere. Statistically significant tropospheric anomalies, for example, a weakening of the Hadley circulation (Figure 7b) and the tropospheric jet (Figures 4b and 7d) as well as significant surface temperature changes (Figure 8), are produced in the model which seem to be lagged to changes in the upper stratosphere by about 2 months.

[37] These model results for the NH are in good agreement with new considerations from observations [e.g., *Kodera and Kuroda*, 2002; *Hood*, 2004]. Further *Randel et al.* [2002] show that the EPF divergence due to extratropical waves determines the zonal mean temperatures in the tropical lower stratosphere. *Hood* [2004] reports a decadal modulation of extratropical wave forcing due to the 11-year solar cycle which further influences lower stratospheric temperatures. For the model experiments the change in the extratropical wave forcing mainly determines the temperature changes in the lower stratosphere in January and confirms in this respect the recent findings from observations.

[38] It should be pointed out that GCM studies so far have failed to produce such a good correspondence with the observed magnitude and temporal evolution of the zonal wind anomalies in NH winter [*Matthes et al.*, 2003]. Only *Shindell et al.* [1999, 2001] could reproduce a limited poleward downward propagation of the zonal wind anomalies.

[39] The improved solar signal during NH winter is related to the relaxation toward realistic wind profiles throughout the stratosphere. An earlier experiment with the same model and the same radiation and ozone changes but an artificially prescribed QBOw only in the equatorial lower stratosphere failed to reproduce the observed QBO-Sun relationship and the magnitude and evolution of the signal [*Labitzke and Matthes*, 2003]. Therefore the improvement of the presented simulations can be ascribed to the implementation of more realistic equatorial winds which seems to be essential in the upper stratosphere. The SAO in the model is more realistic and the mean zonal wind field in the subtropics becomes closer to observations. During October when the SAO is in its west phase the prescribed equatorial winds produce additional weak westerlies around the equatorial stratopause leading to a stronger SAOw phase, a more equatorward movement of the PNJ and hence to an improved climatological wind field (not explicitly shown). The weak westerlies in the upper stratosphere allow planetary waves to propagate more equator-

ward and probably enabled an improved treatment of the relatively weak solar signal. However, the SAOw phase in the model is still about 10 m s^{-1} weaker than in observations (Figures 2b and 2c). This might explain the weaker modeled solar signal in early winter hence the weaker initial westerly wind anomaly. The former experiments [*Labitzke and Matthes*, 2003] displayed a very weak SAOw and a very strong SAOe phase which probably suppressed the weak solar signal. Thus we conclude that the existence of a realistic stratospheric SAO in the FUB-CMAM is at least partly responsible for the good agreement between modeled and observed patterns. A realistic reproduction of the climatological mean circulation as well as the observed interannual variability has been shown to be important for a successful GCM simulation [*Kodera et al.*, 2003].

[40] The relaxation toward equatorial wind profiles for QBOe (QBOw) conditions was exactly the same for solar max and solar min conditions. Any changes at the equator can therefore arise either from solar irradiance changes or internal variability. During solar max years both SAO phases are stronger, especially the SAOw phase in October and the SAOe phase in January. This effect is especially evident for the QBOe experiment whereas only a weak influence on the SAO phases is detected for the QBOw experiment (not shown). A stronger SAOw phase under solar max conditions was also seen in observations [*Nastrom and Belmont*, 1980; *Hood*, 2004].

[41] Despite the improvement of the NH winter signal, the NH summer signal as well as the signals during SH winter and summer (not shown) are still very small. The small SH winter signal is probably due to the excessively strong modeled PNJ which suppresses the weak initial solar signal in early winter and planetary wave propagation in general. The strong SH PNJ was also assumed to be responsible for the weak NH summer signal which is thought to be controlled via MMC changes from the winter hemisphere.

[42] Compared to observations the solar signal in the model is especially smaller at low latitudes which might arise from the steady relaxation toward an equatorial wind profile neglecting the realistic phase change of the QBO as well as the downward propagation of the shear zones. Other above discussed assumptions, for example, the fixed ozone changes, could also be responsible for the missing variability at low latitudes.

6. Summary

[43] Despite the discussed uncertainties in the GCM and the observations the presented results display an important improvement of the simulated solar signal in the NH winter season. The model experiments have confirmed the results of recent observational and model studies [*Gray et al.*, 2001a, 2001b] which suggested the importance of upper stratospheric winds for the NH winter evolution. By imposing more realistic equatorial winds throughout the stratosphere, the model produces a more realistic response of the PNJ and the MMC to the solar cycle influence, similar to that shown by *Kodera and Kuroda* [2002] and *Hood* [2004]. The improvement of the modeled solar signal during the dynamically active season at high northern latitudes was ascribed to a better wind climatology due to the imposed relaxation toward realistic equatorial winds, allowing a more realistic feedback of the weak solar signal. On the other hand, the poor SH wind climatology is probably responsible for the missing solar signal during SH winter as well as for the weak NH summer signal. The magnitude of the simulated anomalies is weaker than in observations which is especially evident at low latitudes and during summer.

[44] The solar signal from the upper stratosphere influences tropospheric circulation patterns in the model as suggested from observations. A more detailed investigation of the tropospheric influence and the QBO-Sun interaction will however be subject of a future study.

[45] **Acknowledgments.** We thank J. Lean and J. Haigh for kindly providing the spectral solar irradiance and the ozone change data. We thank M. Kunze for the development and maintenance of the diagnostic programs and two anonymous reviewers for valuable comments. This study has been funded by the European Commission under the contract EVK2-CT-1999-00001 (SOLICE), the German Ministry of Education and Research under the number 01LG0001 (MESA) and by the Grant-in-Aid for Scientific Research of the Japanese Ministry of Education, Culture, Sports, Science and Technology. The GCM integrations and diagnostics were performed on the CRAY J932/16-8192 at the Konrad-Zuse-Zentrum für Informationstechnik Berlin (ZIB).

References

Balachandran, N., and D. Rind (1995), Modeling the effects of UV variability and the QBO on the troposphere-stratosphere system. part I: The Middle Atmosphere, *J. Clim.*, *8*, 2058–2079.

Balachandran, N. K., D. Rind, P. Lonergan, and D. T. Shindell (1999), Effects of solar cycle variability on the lower stratosphere and the troposphere, *J. Geophys. Res.*, *104*, 27,321–27,339.

Baldwin, M. P., and T. J. Dunkerton (2001), Stratospheric harbingers of anomalous weather regimes, *Science*, *294*, 581–584.

Baldwin, M. P., et al. (2001), The Quasi-Biennial Oscillation, *Rev. Geophys.*, *39*, 179–229.

Bates, J. R. (1981), A dynamical mechanism through which variations in solar ultra violet radiation can influence tropospheric climate, *J. Geophys. Res.*, *104*, 27,321–27,339.

Brasseur, G. (1993), The response of the middle atmosphere to long-term and short-term solar variability: A two-dimensional model, *J. Geophys. Res.*, *98*, 23,079–23,090.

Charney, J. G., and P. G. Drazin (1961), Propagation of planetary-scale disturbances from the lower into the upper atmosphere, *J. Geophys. Res.*, *66*, 83–109.

Christiansen, B. (2001), Downward propagation of zonal mean zonal wind anomalies from the stratosphere to the troposphere: Model and reanalysis, *J. Geophys. Res.*, *106*, 27,307–27,322.

Cubasch, U., G. C. Hegerl, R. Voss, J. Waszkewitz, and T. C. Crowley (1997), Simulation with an O-AGCM of the influence of variations of the solar constant on the global climate, *Clim. Dyn.*, *13*, 757–767.

Dunkerton, T. J., D. P. Delisi, and M. P. Baldwin (1998), Middle atmosphere cooling trend in historical rocketsonde data, *Geophys. Res. Lett.*, *25*, 3371–3374.

Fleming, E. L., S. Chandra, C. H. Jackmann, D. B. Considine, and A. R. Douglass (1995), The middle atmosphere response to short and long term solar UV variations: Analysis of observations and 2D model results, *J. Atmos. Terr. Phys.*, *57*, 333–365.

Fortuin, J. P. F., and U. Langematz (1994), An update on the global ozone climatology and on concurrent ozone and temperature trends, SPIE *Atmospheric Sensing and Modeling, 29–30 September 1994, Rome, Italy*, edited by R. P. Santer, pp. 207–216, SPIE-Int. Soc. for Opt. Eng., Bellingham, Wash.

Garcia, R. R., and F. Sassi (1999), Modulation of the mesospheric semiannual oscillation by the Quasibiennial Oscillation, *Earth Planets Space*, *51*, 563–569.

Garcia, R. R., T. J. Dunkerton, R. S. Lieberman, and R. A. Vincent (1997), Climatology of the semiannual oscillation of the tropical middle atmosphere, *J. Geophys. Res.*, *102*, 26,019–26,032.

Giorgetta, M. A., E. Manzini, and E. Roeckner (2002), Forcing of the Quasi-Biennial Oscillation from a broad spectrum of atmospheric waves, *Geophys. Res. Lett.*, *29*(8), 1245, doi:10.1029/2002GL014756.

Gleisner, H., and P. Thejll (2003), Patterns of tropospheric response to solar variability, *Geophys. Res. Lett.*, *30*(13), 1711, doi:10.1029/2003GL017129.

Gray, L. J., E. F. Drysdale, T. J. Dunkerton, and B. N. Lawrence (2001a), Model studies of the interannual variability of the Northern Hemisphere stratospheric winter circulation: The role of the Quasi Biennial Oscillation, *Q. J. R. Meteorol. Soc.*, *127*, 1413–1432.

Gray, L. J., S. J. Phipps, T. J. Dunkerton, M. P. Baldwin, E. F. Drysdale, and M. R. Allen (2001b), A data study of the influence of the equatorial upper stratosphere on Northern Hemisphere stratospheric sudden warmings, *Q. J. R. Meteorol. Soc.*, *127*, 1985–2003.

Haigh, J. D. (1994), The role of stratospheric ozone in modulating the solar radiative forcing of climate, *Nature*, *370*, 544–546.

Haigh, J. D. (1996), The impact of solar variability on climate, *Science*, *272*, 981–984.

Haigh, J. D. (1999), A GCM study of climate change in response to the 11-year solar cycle, *Q. J. R. Meteorol. Soc.*, *125*, 871–892.

Holton, J. R., and H. Tan (1980), The influence of the equatorial Quasi-Biennial Oscillation on the global circulation at 50 mb, *J. Atmos. Sci.*, *37*, 2200–2208.

Holton, J. R., and H. Tan (1982), The Quasi-Biennial Oscillation in the Northern Hemisphere lower stratosphere, *J. Meteorol. Soc. Jpn.*, *60*, 140–148.

Hood, L. L. (2004), Effects of solar UV variability on the stratosphere, in *Solar Variability and Its Effect on the Earth's Atmospheric and Climate System*, *Geophys. Monogr. Ser.*, edited by J. Pap et al., AGU, Washington, D. C., in press.

Hood, L. L., J. L. Jirikowic, and J. P. McCormack (1993), Quasi-decadal variability of the stratosphere: Influence of long-term solar ultraviolet variations, *J. Atmos. Sci.*, *50*, 3941–3958.

Kodera, K. (2002), Solar cycle modulation of the North Atlantic Oscillation: Implication in the spatial structure of the NAO, *Geophys. Res. Lett.*, *29*(8), 1218, doi:10.1029/2001GL014557.

Kodera, K., and Y. Kuroda (2002), Dynamical response to the solar cycle, *J. Geophys. Res.*, *107*(D24), 4749, doi:10.1029/2002JD002224.

Kodera, K., and K. Yamazaki (1990), Long-term variation of upper stratospheric circulation in the Northern Hemisphere in December, *J. Meteorol. Soc. Jpn.*, *68*, 101–105.

Kodera, K., K. Yamazaki, M. Chiba, and K. Shibata (1990), Downward propagation of upper stratospheric mean zonal wind perturbation to the troposphere, *Geophys. Res. Lett.*, *17*, 1263–1266.

Kodera, K., M. Chiba, and K. Shibata (1991), A general circulation model study of the solar and QBO modulation of the stratospheric circulation during Northern Hemisphere winter, *Geophys. Res. Lett.*, *18*, 1209–1212.

Kodera, K., K. Matthes, K. Shibata, U. Langematz, and Y. Kuroda (2003), Solar impact on the lower mesospheric subtropical jet in winter: A comparative study with general circulation model simulations, *Geophys. Res. Let.*, *30*(D6), 1315, doi:10.1029/2002GL016124.

Kuroda, Y., and K. Kodera (2002), Effect of solar activity on the polar-night jet oscillation in the Northern and Southern Hemisphere winter, *J. Meteorol. Soc. Jpn.*, *80*, 973–984.

Labitzke, K. (1987), Sunspots, the QBO and the stratospheric temperature in the north polar region, *Geophys. Res. Lett.*, *14*, 535–537.

Labitzke, K. (2001), The global signal of the 11-year sunspot cycle in the stratosphere: Differences between solar maxima and minima, *Meteorol. Z.*, *10*, 901–908.

Labitzke, K. (2002), The solar signal of the 11-year sunspot cycle in the stratosphere: Differences between the northern and southern summers, *J. Meteorol. Soc. Jpn.*, *80*, 963–971.

Labitzke, K. (2003), The global signal of the 11-year sunspot cycle in the atmosphere: When do we need the QBO?, *Meteorol. Z.*, *12*, 209–216.

Labitzke, K., and K. Matthes (2003), 11-year solar cycle variations in the atmosphere: Observations, mechanisms, and models, *Holocene*, *13*, 311–317.

Labitzke, K., and H. van Loon (1988), Associations between the 11-year solar cycle, the QBO and the atmosphere, part I: The troposphere and stratosphere in the Northern Hemisphere in winter, *J. Atmos. Terr. Phys.*, *50*, 197–206.

Labitzke, K., J. Austin, N. Butchart, J. Knight, M. Takahashi, M. Nakamoto, T. Nagashima, J. Haigh, and V. Williams (2002), The global signal of the 11-year solar cycle in the stratosphere: Observations and model results, *J. Atmos. Terr. Phys.*, *64*, 203–210.

Langematz, U. (2000), An estimate of the impact of observed ozone losses on stratospheric temperatures, *Geophys. Res. Lett.*, *27*, 2077–2080.

Langematz, U., and S. Pawson (1997), The Berlin troposphere-stratosphere-mesosphere GCM: Climatology and forcing mechanisms, *Q. J. R. Meteorol. Soc.*, *123*, 1075–1096.

Larkin, A., J. D. Haigh, and S. Djavidnia (2000), The effect of solar UV radiation variations on the Earth's atmosphere, *Space Sci. Rev.*, *94*, 199–214.

Lean, J. L., G. J. Rottman, H. L. Kyle, T. N. Woods, J. R. Hickey, and L. C. Puga (1997), Detection and parameterisation of variations in solar mid- and near-ultraviolet radiation (200–400 nm), *J. Geophys. Res.*, *102*, 29,939–29,956.

Lee, H., and A. K. Smith (2003), Simulation of the combined effects of solar cycle, Quasi-Biennial Oscillation, and volcanic forcing on stratospheric ozone changes in recent decades, *J. Geophys. Res.*, *108*(D2), 4049, doi:10.1029/2001JD001503.

Matthes, K., K. Kodera, J. D. Haigh, D. T. Shindell, K. Shibata, U. Langematz, E. Rozanov, and Y. Kuroda (2003), GRIPS solar experiments intercomparison project: Initial results, *Pap. Meteorol. Geophys.*, *54*, 71–90.

Morcrette, J. J. (1991), Radiation and cloud radiative properties in the European Centre for Medium-Range Weather Forecasts forecasting system, *J. Geophys. Res.*, *96*, 9121–9132.

Müller, K. M., U. Langematz, and S. Pawson (1997), The stratopause semiannual oscillation in the Berlin troposphere-stratosphere-mesosphere GCM, *J. Atmos. Sci.*, *54*, 2749–2759.

Nastrom, G. D., and A. D. Belmont (1980), Apparent solar cycle influence on long-period oscillations in stratospheric zonal wind speed, *Geophys. Res. Lett.*, *7*, 457–460.

Pap, J. M. (2003), Total solar and spectral irradiance variations from near-UV to infrared, in *The Variable Shape of the Sun: Astrophysical Consequences, Lecture Notes in Physics*, edited by J. P. Rozelot, pp. 129–158, Springer-Verlag, New York.

Pawson, S., U. Langematz, G. Radek, U. Schlese, and P. Strauch (1998), The Berlin troposphere-stratosphere-mesosphere GCM: Sensitivity to physical parameterizations, *Q. J. R. Meteorol. Soc.*, *124*, 1343–1371.

Pawson, S., et al. (2000), The GCM-reality intercomparison project for SPARC (GRIPS): Scientific issues and initial results, *Bull. Am. Meteorol. Soc.*, *81*, 781–796.

Pittock, B. A. (1978), A critical look at long-term Sun-weather relationships, *Rev. Geophys.*, *16*, 400–420.

Randel, W. J., R. R. Garcia, and F. Wu (2002), Time-dependent upwelling in the tropical lower stratosphere estimated from the zonal-mean momentum budget, *J. Atmos. Sci.*, *59*, 2141–2152.

Rind, D., P. Lonergan, N. K. Balachandran, and D. Shindell (2002), $2 \times CO_2$ and solar variability influences on the troposphere through wave-mean flow interactions, *J. Meteorol. Soc. Jpn.*, *80*, 863–876.

Salby, M., and P. Callaghan (2000), Connection between the solar cycle and the QBO: The missing link, *J. Clim.*, *13*, 2652–2662.

Scaife, A. A., J. Austin, N. Butchart, S. Pawson, M. Keil, J. Nash, and I. N. James (2000), Seasonal and interannual variability of the stratosphere diagnosed from UKMO TOVS analyses, *Q. J. R. Meteorol. Soc.*, *126*, 2585–2604.

Shindell, D., D. Rind, N. Balachandran, J. Lean, and J. Lonergan (1999), Solar cycle variability, ozone, and climate, *Science*, *284*, 305–308.

Shindell, D. T., G. A. Schmidt, R. L. Miller, and D. Rind (2001), Northern Hemisphere winter climate response to greenhouse gas, ozone, solar, and volcanic forcing, *J. Geophys. Res.*, *106*, 7193–7210.

Shine, K. P., and J. A. Rickaby (1989), Solar radiative heating due to the absorption by ozone, in *Ozone in the Atmosphere*, edited by R. D. Bojkov and P. Fabian, pp. 597–600, A. Deepak, Hampton, Va.

Strobel, D. F. (1978), Parameterization of the atmospheric heating rate from 15 to 120 km due to O_2 and O_3 absorption of solar radiation, *J. Geophys. Res.*, *83*, 6225–6230.

Svensmark, H., and E. Friis-Christensen (1997), Variation of cosmic ray flux and global cloud coverage—A missing link in solar-climate relationships, *J. Atmos. Terr. Phys.*, *59*, 1225–1232.

Thompson, D. W. J., and J. M. Wallace (1998), The Arctic Oscillation signature in the wintertime geopotential height and temperature fields, *Geophys. Res. Lett.*, *25*, 1297–1300.

Tourpali, K., C. J. E. Schuurmans, R. van Dorland, B. Steil, and C. Brühl (2003), Stratospheric and tropospheric response to enhanced solar UV-radiation: A model study, *Geophys. Res. Lett.*, *30*(5), 1231, doi: 10.1029/2002GL016650.

Wetherald, R. T., and S. Manabe (1975), The effects of changing the solar constant on the climate of a general circulation model, *J. Atmos. Sci.*, *32*, 2044–2059.

White, W. R., J. Lean, D. R. Cayan, and M. D. Dettinger (1997), Response of global upper ocean temperature to changing solar irradiance, *J. Geophys. Res.*, *102*, 3255–3266.

World Meteorological Organization (1986), Atmospheric ozone 1985, *Global Ozone Res. Monit. Proj. Rep. 16/1*, Geneva.

L. L. Gray, Centre for Global Atmospheric Modelling, Meteorology Department, Reading University, Earley Gate, PO Box 243, Reading RG6 6BB, UK.

K. Kodera, Meteorological Research Institute, 1-1, Nagamine, Tsukuba, Ibaraki, 305-0052 Japan.

K. Labitzke, U. Langematz, and K. Matthes, Institut für Meteorologie, Freie Universität Berlin, Carl-Heinrich-Becker Weg 6-10, 12165 Berlin, Germany. (matthes@strat01.met.fu-berlin.de)